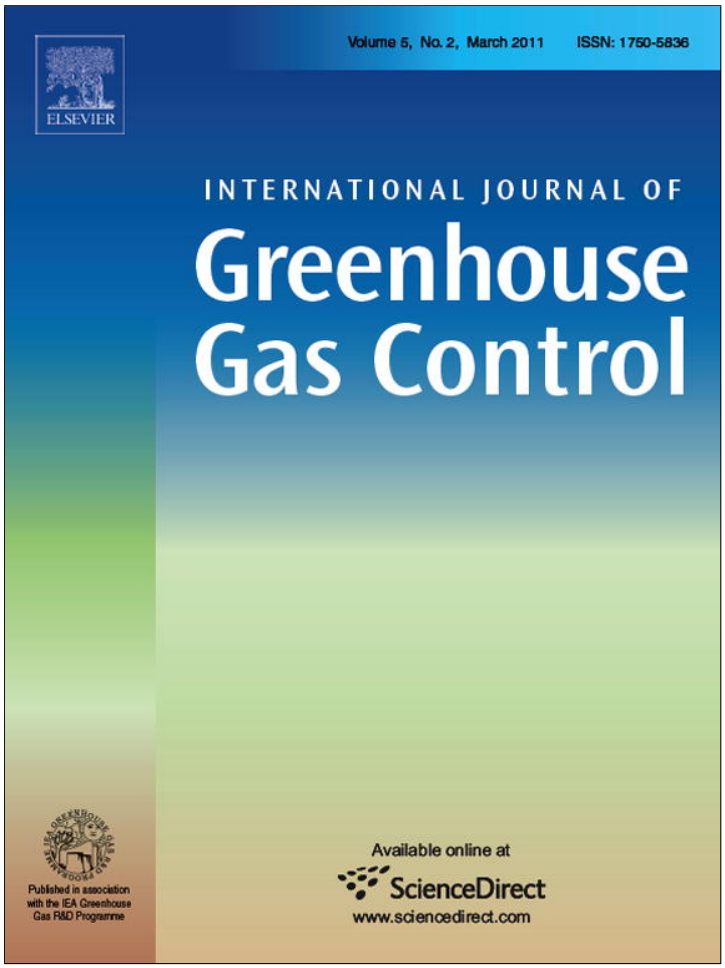

International Journal of Greenhouse Gas Control 5 (2011) 347–355

Contents lists available at ScienceDirect

International Journal of Greenhouse Gas Control

journal homepage: www.elsevier.com/locate/ijggc

Evolution of hydrogen sulfide in sour saline aquifers during carbon dioxide sequestration

Seyyed M. Ghaderi [a], David W. Keith [a], Rob Lavoie [b], Yuri Leonenko [c,*]

[a] Department of Chemical and Petroleum Engineering, University of Calgary, Calgary, Alberta, Canada T2N 1N4
[b] CalPetra Research and Consulting Inc., Calgary, Alberta, Canada T2R 0B8
[c] Department of Physics, University of Waterloo, Waterloo, Ontario, Canada N2L 3G1

ARTICLE INFO

Article history:
Received 21 July 2009
Received in revised form 8 September 2010
Accepted 25 September 2010
Available online 30 October 2010

Keywords:
Acid gas injection
CO_2 sequestration
Compositional simulation
H_2S exsolution
Sour saline aquifer

ABSTRACT

Many deep saline aquifers suitable for carbon dioxide (CO_2) sequestration contain measurable concentrations of hydrogen sulfide (H_2S). These aquifers are described here as *sour saline aquifers* and the other ones as *ordinary saline aquifers*. Sour saline aquifers occur wherever even minor amounts of anhydrite or other sulfate sources are present in the formation. In this paper, compositional modeling of CO_2 injection into such aquifers is studied. When CO_2 is injected into a sour saline aquifer, the H_2S initially dissolved in the brine will be exsolved and released into an expanding CO_2 plume. At any time after the start of CO_2 injection, the region swept by the plume consists of two sub-regions. The first of these is an inner sub-region extending from the injection well, and is characterized by the absence of H_2S in both aqueous and gaseous phases. The dissolved H_2S in this inner sub-region is nearly completely removed from the brine via an exsolution process. The second sub-region extends from the outer edge of the inner sub-region to the leading edge of the plume. In this outer sub-region, the mole fraction of H_2S in the gas plume gradually increases toward the leading edge and reaches a peak value. While the gas plume is expanding the size of the outer sub-region enlarges. Following the discussion of these phenomena, in the next part of the paper, injection of acid gases (mixtures of H_2S and CO_2) into sour saline aquifers and ordinary saline aquifers is explored. In contrast to sour aquifers, unsaturated water in an ordinary aquifer will strip away H_2S from the CO_2 stream and consequently the mole fraction of H_2S toward the gas front decreases. The highly toxic nature of H_2S gas suggests the need to account for dissolved H_2S in sour saline aquifers when establishing risk assessment, monitoring, and management strategies at CO_2 storage sites.

1. Introduction

Carbon dioxide emissions arising from use of fossil fuels are likely to be the dominant drivers of climate change over the coming century (IPCC, 2007). The use of carbon dioxide capture and geologic storage (usually known as CCS) offers the possibility of maintaining access to fossil energy while reducing emissions of carbon dioxide to the atmosphere. Injection of nearly pure CO_2 and also injection of acid gas (CO_2 and H_2S) may occur over a wide range of aquifer and reservoir characteristics and operating conditions (Bachu and Gunter, 2005). For acid gas injection, the composition of the injected gas can vary widely. To the end of 2003, close to 2.5 Mt CO_2 and 2.0 Mt H_2S (in different composition streams) have been injected into deep saline aquifers and depleted reservoirs in Western Canada at average rates that vary between 1×10^3 and 5×10^5 m^3/day (Bachu and Gunter, 2005).

Several studies have reported the numerical simulation of the CO_2 storage process, usually in order to establish more efficient schemes to store larger volumes of gas (e.g., Kumar et al., 2005; Leonenko and Keith, 2008). Moreover, different aspects of acid gas disposal in saline aquifers have been investigated in recent years (e.g., Adams and Bachu, 2002; Carrol, 2002a,b; Bachu and Carroll, 2005; Bennion and Bachu, 2008). Although some studies have assessed the implications of impurities in the injection stream (Ozah et al., 2005; Bachu and Bennion, 2009; Bachu et al., 2009; Battistelli and Marcolini, 2009), scant attention has been paid to investigating the consequences of injecting CO_2 or acid gas into formations that contain pre-existing impurities in the in-situ brine of the target formation.

Some authors have addressed the presence of gases dissolved in saline aquifers where CO_2 sequestration is planned. The Frio brine formation in the U.S. is believed to be nearly saturated with methane (Doughty et al., 2004; Hovorka et al., 2004) and the

* Corresponding author. Tel.: +1 519 888 4567x32160; fax: +1 519 748 8115.
E-mail addresses: leonenko@uwaterloo.ca, leonenko@uwaterloo.ca (Y. Leonenko).

1750-5836/$ – see front matter © 2010 Elsevier Ltd. All rights reserved.
doi:10.1016/j.ijggc.2010.09.008

Table 1
Parameters used in Eq. (2) to calculate Henry's constants for CO_2 and H_2S at different pressures.

Component	Parameters in Eq. (1)	Fresh water	Saline brine
CO_2	H^0 (kPa)	3.21E+5	4.5E+5
	V^* (l mole^{-1})	3.55E−2	3.52E−2
	P^0 (kPa)	0.0	0.0
H_2S	H^0 (kPa)	1.28E+5	1.60E+5
	V^* (l mole^{-1})	3.59E−2	3.56E−2
	P^0 (kPa)	0.0	0.0

Nisku brine formation in Canada contains measurable amounts of dissolved H_2S (Hutcheon, 1999). In addition, the occurrence of non-hydrocarbon gases (CO_2, H_2S, He, and N_2) is quite common in strata of all ages in the Alberta Basin which is a part of the Western Canada Sedimentary Basin (Hutcheon, 1999). The Rocky Mountains and the Appalachians in North America, where CO_2 injection and geological storage on a large scale is most likely to be implemented in Canada and the United States (Bachu and Gunter, 2005), are among these formations. Battistelli and Marcolini (2009) have shown the exsolution of dissolved CH_4 and its accumulation at the edge of the CO_2 plume during a sequestration process.

In this study, a commercial compositional reservoir simulator, CMG-GEM™ version 2008.12, is used to perform the numerical simulation of CO_2 injection into a saline aquifer that initially contains H_2S as an impurity in the in-situ fluid. Although the aquifer's brine may contain several impurities (Ahmed, 1989; Hutcheon, 1999), the focus of this paper is to study the effect of H_2S impurity on the CO_2 storage efficiency, due to the toxic nature of H_2S and high likelihood of its occurrence. Different scenarios for injecting CO_2 either as a single component gas or as a mixture with H_2S as an additional component (i.e., an acid gas comprised of 80% CO_2 and 20% H_2S) was considered.

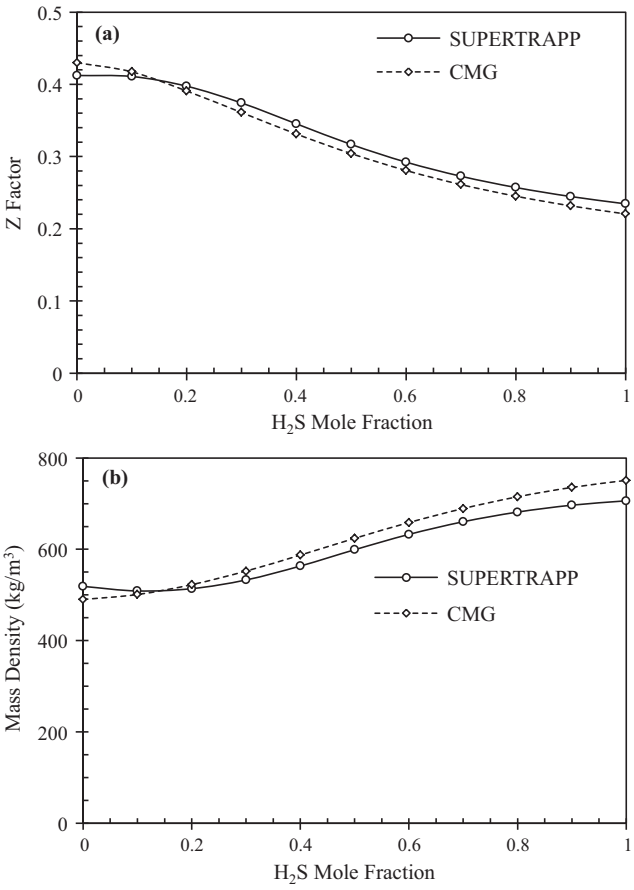

Fig. 1. Comparison between SUPERTRAPP and CMG predictions for H_2S–CO_2 binary mixtures at 61 °C and 13,500 kPa for Z factor (a) and mass density (b) as a function of mole fraction of hydrogen sulfide.

2. Model

2.1. Fluid representation in CMG-GEM

The dissolution and exsolution of gaseous components in and from the aqueous phase (water or brine) is calculated in the CMG-GEM model using the general Henry's law (Li and Nghiem, 1986):

$$f_i = x_i H_i \tag{1}$$

in which f_i is the fugacity of component i in the gaseous phase, x_i is its mole fraction in the aqueous phase and H_i is the Henry's law constant of the component. Pressure and temperature dependence of the Henry's constant for each component (H (kPa)) is expressed by (Computer Modelling Group, 2008):

$$\ln(H) = \ln(H^0) + \frac{V^*(P - P^0)}{RT} \tag{2}$$

where H^0 (kPa) is the reference Henry's constant at the reference pressure P^0 (kPa), V^* is the partial molar volume of the component at infinite dilution (l mole^{-1}), P is the pressure (kPa), T is the temperature (K) and R is the universal gas constant (8.314 kPa l mole^{-1} K^{-1}). The greater the value of Henry's constant for a given component, the less soluble it is in the aqueous phase. Table 1 shows the set of parameters required for calculating the Henry's constants for CO_2 and H_2S at different pressures and at a constant temperature equal to 61.0 °C and two different aqueous phase salinities: a brine with zero salinity (fresh water), and a saline brine with salinity equivalent to 118,950 mg NaCl per liter of solution.

The values provided in this table have been verified against experimental data (see Pooladi-Darvish et al. (2009) and Bachu et al. (2009) for more details). The Henry's constants clearly show that solubility of these gaseous components decrease with an increase in salinity of the formation brine. The Peng–Robinson Equation of State (1976) is used along with Eq. (2) to model the fugacity of components required in Henry's law. GEM provides that, at initial pressure (13,500 kPa), temperature (61 °C), and salinity (118,950 mg l^{-1}), it is possible to dissolve 0.02 H_2S by mole fraction into the brine which is equivalent to a 1.14 molal solution.

Fig. 1a and b shows CMG calculated Z factor and mass density, respectively, at fixed pressure and temperature for binary mixtures of H_2S–CO_2 as functions of H_2S mole fraction. CMG predictions are compared to calculations performed using the computer program SUPERTRAPP (NIST, 2007) and show acceptable accuracy and consistency. These figures illustrate the smooth change in properties of the CO_2–H_2S binary mixtures as the mole fraction of H_2S increases. Therefore, at pressures greater than the critical pressure of all possible binary mixtures of H_2S and CO_2 (which is the case in the present simulations), using a single phase approach for these mixtures of varying composition is valid. In this study, this single phase is called either a gas phase or more generally a non-aqueous phase.

CMG predictions for P-T diagrams of this binary system have been displayed in Fig. 2a. This figure also shows the initial pressure and temperature of the aquifer. Since the variation in the viscosity of the CO_2–H_2S mixtures in the composition range applicable for this study was not considerable (see Fig. 2b), the viscosity of the non-aqueous phase mixtures was taken as a constant value equal to 0.05 cp. Using this average value in comparison with the highest and lowest values gives rise to only a 5% error in estimating plume extension. Viscosity of the brine was calculated according to Bachu and Carroll (2005) and for fresh water that same viscosity was used.

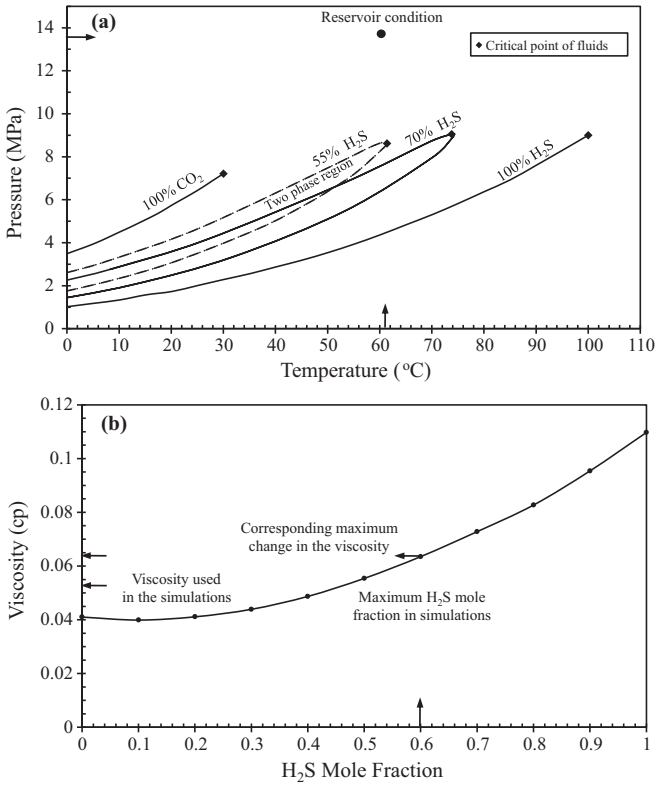

Fig. 2. (a) P-T diagram of H_2S–CO_2 mixtures at four different compositions. The pressure and temperature of the reservoir has also been indicated; (b) viscosity of H_2S–CO_2 mixtures at reservoir condition (61 °C and 13,500 kPa) as predicted by SUPERTRAPP which shows the small variation of viscosity between pure CO_2 and a mixture consisting of 0.6 H_2S by mole fraction.

2.2. Main features of simulation models

All simulations were performed in a one-dimensional radial model, with an absolute permeability of 5000 mD, a porosity of 30%, a radius of 100 m, and a thickness of 1.0 m (see Table 2 for a full list of aquifer properties).

The initial pressure, temperature, and salinity of the brine are the same as the values that were used in the numerical simulations by Bachu et al. (2009). The relative permeability curves were characterized using the Corey correlation (1954) with exponents of 2.0 and 1.5 for the gas and water relative permeability curves, respectively. Fig. 3 presents the curves used in the simulations. The residual brine saturation was set equal to 0.1, and two different end point relative permeability values for the gas phase of 0.4 and 1.0 were considered for the Base Case and one sensitivity analysis, respectively.

Table 2
Properties of aquifer and fluids and injection details for the Base Case simulation.

Radius (m)	100
Thickness (m)	1.0
Absolute permeability (mD)	5000
Porosity	0.30
Rock compressibility (kPa^{-1})	5.0E−7
Temperature (°C)	61.0
Initial pressure (kPa)	13,500
Brine salinity ($mg\,l^{-1}$)	118,950
Initial mole fraction of dissolved H_2S	0.02
Grid system	1D-radial
n_r	2000
Aqueous phase viscosity (cp)	0.58
Non-aqueous phase viscosity (cp)	0.05
Injection gas composition	Pure CO_2
Injection rate (rm^3/day)	4.0
Injection period (days)	100

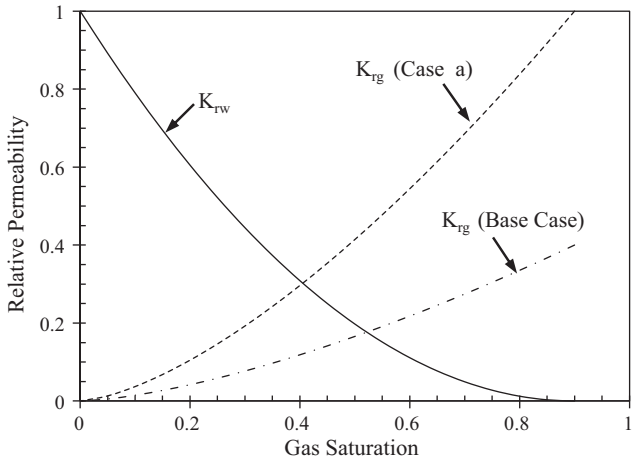

Fig. 3. Water–gas relative permeability curves.

The model employed a single vertical injection well with constant injection rate constraint at the center of a bounded radial model, and was accompanied with a production well at the boundary to mimic a constant pressure boundary condition. Injection simulations of pure CO_2 and an 80% CO_2–20% H_2S mixture at supercritical conditions were performed for 100 days. The injection rate was fixed at 4.0 rm^3/day (≈1100 sm^3/day). The high value of absolute permeability and injection rate ascertain the proper propagation of the gas plume at a reasonable time while producing minimum pressure disturbance in the models.

It is worth mentioning some of the other relevant features and assumptions of the simulation models. First, GEM is an isothermal simulator in which the temperature of the injected fluids as well as the temperature of the reservoir remains constant at the user specified value, thereby neglecting all possible thermal effects. Second, true representation of the reservoir in the z direction may require using a multi-layered system which can capture any possible gravity segregation and hence saturation distribution. However, to reduce the degree of complexity of the problem, one layered system was used. Third, although the molecular diffusion can play a role when there is a concentration gradient and also can cause back-mixing of the dissolved components with the (newly) injected gas, it was neglected in the current study. Fourth, the vaporization of water and related side effects such as formation dry-out, salt precipitation, and reductions in permeability and porosity (Pruess, 2009; Zeidouni et al., 2009) were ignored. This further implies that the water component is only present in the aqueous phase and not in the non-aqueous phase. At the temperature and pressure of interest in this study, the ultimate mole fraction of water in the non-aqueous phase cannot exceed 2–3% (Li and Firoozabadi, 2009). Fifth, the capillary pressure was not considered in this study.

3. Results and discussion

3.1. Preliminary simulation results

The preliminary simulation results indicated that injection of pure CO_2 into a saline aquifer which is initially saturated with H_2S (Table 2) causes the exsolution and release of dissolved H_2S into the expanding CO_2 plume. Moreover, the expanding CO_2 plume (or acid gas plume) delivers all of the exsolved H_2S progressively towards the leading edge of the plume.

The effect of discretization on solution accuracy was investigated by conducting simulations with different degrees of

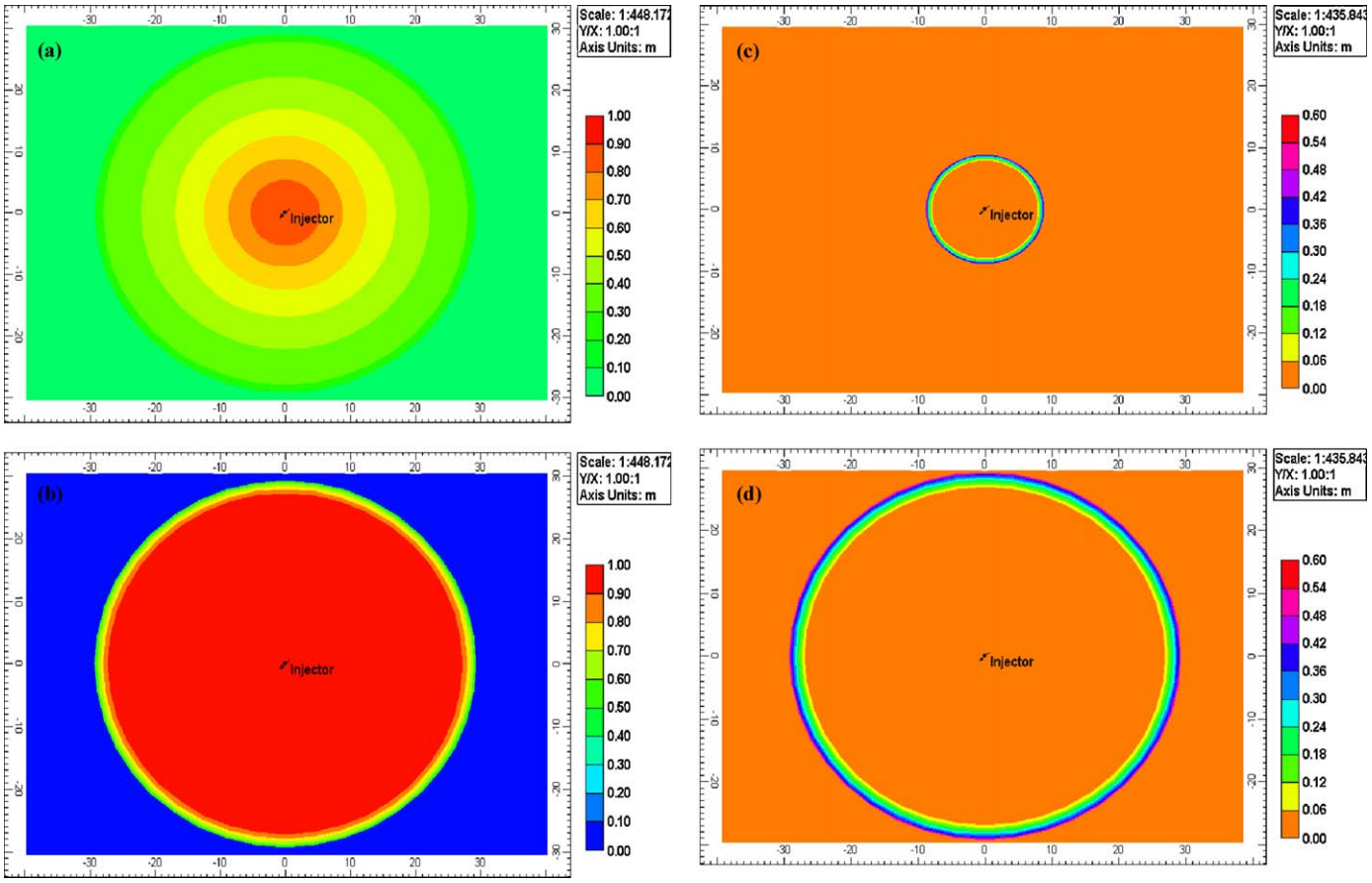

Fig. 4. Simulation results: (a) gas saturation profile after 100 days; (b) CO_2 mole fraction in the gas phase ($y^g_{CO_2}$) after 100 days (note that the mole fraction of H_2S ($y^g_{H_2S}$) at any location is equal to $1.0 - y^g_{CO_2}$); (c) variation of H_2S mole fraction in the gas phase after 10 days; (d) variation of H_2S mole fraction in the gas phase after 100 days.

refinement. It was concluded that fine grids are required to accurately capture the gas plume radius at any time, and to evaluate its composition correctly, 2000 grid cells (each 1.0 m thick and 0.05 m of radial extent) were considered for all simulation models to achieve this goal.

Fig. 4a shows the gas saturation variation within the aquifer after 100 days. As can be seen in Fig. 4b, the mole fraction of CO_2 within this plume changes from 1.0 at the point of injection and gradually decreases toward zero close to the outer boundary of the plume. Fig. 4c and d illustrates the variation in the H_2S composition of the plume after 10 days and 100 days, respectively, indicating a substantial increase in the radial extent of the evolved region. Since the plume expansion is symmetrical in the radial models, henceforth 2D graphs will be used to better illustrate the development of gas saturation and H_2S evolution as the gas exsolution progresses.

3.2. Base Case simulation results and observations

As suggested by the above grid sensitivity results, a discretization of 2000 grid cells in the radial direction was chosen as the Base Case. This grid was utilized to investigate the consequences of injection of CO_2 into brine which is saturated with (dissolved) H_2S at the initial conditions described in Table 2. For the Base Case scenario, pure CO_2 is injected at a rate of 4.0 rm^3/day into a vertical well located at the center of the model. As previously described, when the injected CO_2 comes into contact with saturated brine, H_2S progressively exsolves out of the aqueous phase into the gas phase of the advancing CO_2 plume. The CO_2 plume pushes the mobile portion of the brine as well as the exsolved H_2S toward the outer boundary of the domain, while CO_2 continuously dissolves into the brine. According to the simulation results found in this study, at any time after injection starts, the region swept by the plume consists of two sub-regions: an inner radial sub-region extending from the injection well, characterized by the absence of H_2S in both aqueous and non-aqueous phases; and, an outer sub-region, where the mole fraction of H_2S in the gas plume gradually increases towards a peak value at the leading edge. The peak value of H_2S (at the leading edge) is defined by thermodynamic equilibrium at the gas–liquid boundary (based on the fundamental assumption of instantaneous thermodynamic equilibrium which is employed in CMG-GEM calculations). For the ternary system of H_2S–CO_2–H_2O flash calculations indicate that at the temperature, pressure and salinity used in this study, a gas mixture of 54% H_2S and 46% CO_2 is in equilibrium with an aqueous phase consisting of 1.30% H_2S, 0.7% CO_2, and 98% water (all by mole percent). These results of flash calculations are consistent with the experimental results of Bachu et al. (2009) in which they have shown that at the prevailing conditions, the solubility of H_2S is about two times greater than the solubility of CO_2 in aqueous phase. The results of simulations also suggest that the maximum mole fraction of H_2S in gas phase is 0.54 and it is consistent with above data. It should be noted that this result is valid only within assumption and simplification made and discussed previously. It is expected that, if for example the vaporization of water to the gas phase were accounted for, the level of H_2S could proceed to higher values. However, the quantification of such is not the main purpose of this study; instead, emphasis has been placed on the clear understanding of the mechanism involved in the evolution of the very toxic and hazardous H_2S component.

Figs. 5 and 6 show the simulation results for the Base Case scenario after 100 days of injection. From Fig. 5, it is inferred that, after

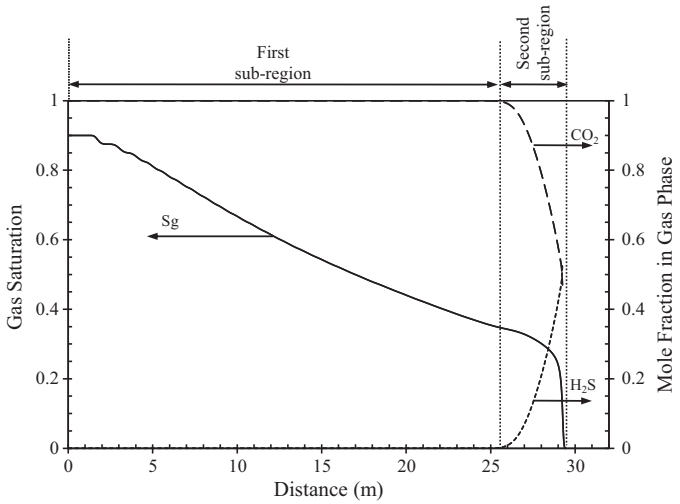

Fig. 5. Development of two sub-regions within the area swept by the CO_2 plume after 100 days of simulation. The solid curve shows the variation of gas saturation versus distance (residual brine saturation is equal to 0.1); the long dashed curve shows the CO_2 mole fraction distribution in the gas phase; the short dashed curve shows the H_2S mole fraction distribution in the gas phase.

100 days, the plume radius will reach approximately 29.3 m. The first sub-region is about 25.8 m in radius, and the second sub-region is about 3.5 m. Fig. 6 clearly shows that the CO_2 has been dissolved into the brine, while H_2S has been exsolved and released into the gas phase. Considering both of these figures together, the occurrence of the equilibrium composition between the two phases (gas and aqueous) at the leading edge is identifiable. As time passes, subsequent to increasing radius of the plume, the extent of the second sub-region which contains a gaseous H_2S concentration also increases. The evolution of H_2S into the gas phase is a dynamic process beginning when CO_2 injection is initiated at the injector. This phenomenon was previously noted and illustrated in Fig. 4c and d.

Fig. 7 shows the gradual development of the outer sub-region. It's width continues to grow and the concept of FWHM (full width at half maximum, δ in Fig. 7) is used to estimate the rate of width growth after stabilization of the peak value, as given by:

$$\frac{\Delta\delta}{\Delta t} = \frac{\delta_2 - \delta_1}{t_2 - t_1} = \frac{1.35 - 1.05}{200 - 100} = 0.003 \quad \left(\frac{\text{m}}{\text{day}}\right) \tag{3}$$

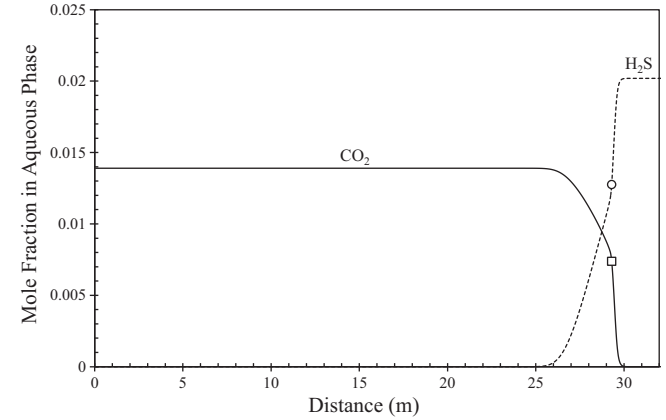

Fig. 6. Variation in the composition of the aqueous phase versus distance in the region swept by the plume after 100 days. The "○" and "□" symbols indicate the equilibrated mole fraction of H_2S and CO_2, respectively, in the aqueous phase in the last block invaded by the gas plume.

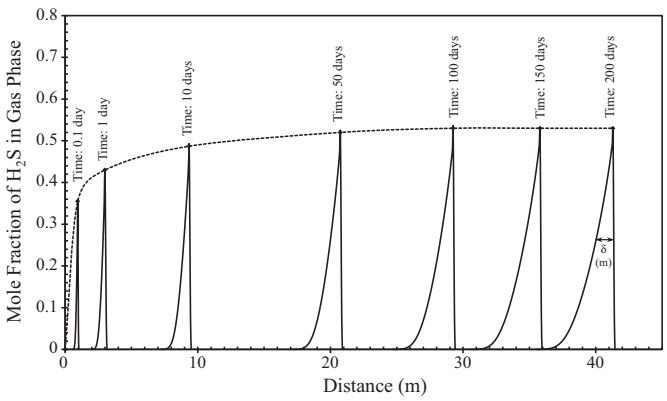

Fig. 7. Mole fraction of H_2S in the gas plume at different times. Maximum observed H_2S mole fraction (dotted line at different times) is about 0.54. Increase in the width of the second region is determined by measuring the characteristic full width at half maximum (FWHM or "δ").

In Eq. (3), δ (m) represents the FWHM of the graphs in Fig. 7 corresponding to times when the peak value has been reached.

One point should be emphasized here. In the vicinity of the injection well in the presence of a strong convective process (strong CO_2 flux) the H_2S concentration gradient is confined within a very thin boundary layer near the edge. The layer's width is increasing from zero (at the well) to scales (far enough from the well) comparable to simulation grid size and at some point the peak value of the layer becomes observable. It happens when dotted line in Fig. 7 starts flattening and equilibrium boundary mole fraction (54%) is clearly present (after 50 days).

From the simulation results, it is also possible to calculate the amount of moles of H_2S in the gas phase at any specific time by evaluating the following integral:

$$n^{\text{g}}_{\text{H}_2\text{S}} = \int_{r_{\text{w}}}^{r_{\text{plume}}} (s_{\text{g}}\rho_{\text{g}}y^{\text{g}}_{\text{H}_2\text{S}}\phi 2\pi hr)dr \tag{4}$$

where $n^{\text{g}}_{\text{H}_2\text{S}}$ (mol) is the moles of gaseous H_2S, s_g is the gas saturation, ρ_g (mol m^{-3}) represents the molar density of the gaseous phase, $y^{\text{g}}_{\text{H}_2\text{S}}$ is the mole fraction of H_2S in the gas phase, ϕ is the porosity, h (m) is the thickness of the reservoir, and r (m) is the radius from the injection well. The integration is carried out over a distance from the wellbore radius (r_w) to the plume radius (r_{plume}). Fig. 8 shows the graph of the integrant in Eq. (4) after 100 days of injection. The amount of H_2S released to the gas phase at this time

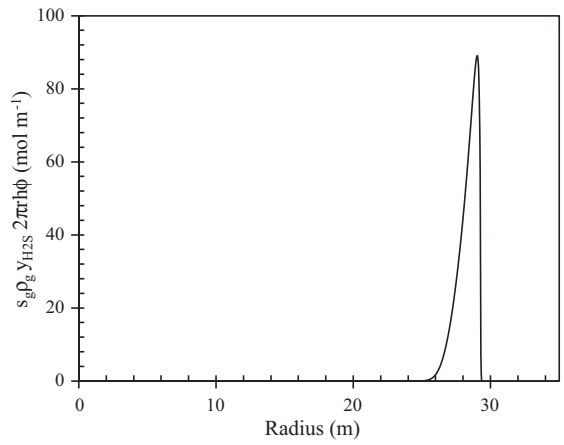

Fig. 8. Moles of H_2S released to the gas phase per unit length versus distance from the injection well after 100 days. At this point in time, the area underneath the curve represents the total amount of H_2S released to the gas phase.

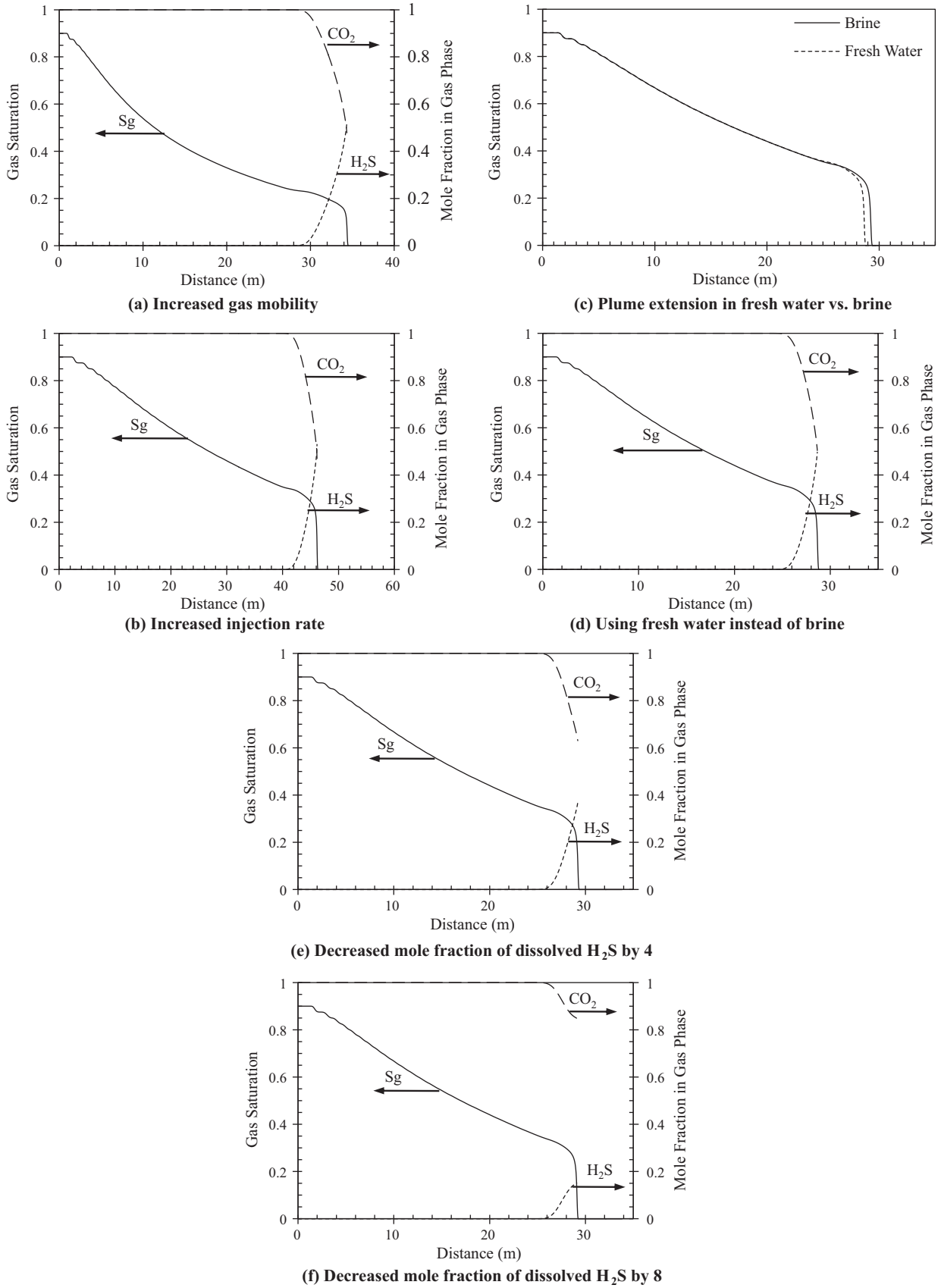

Fig. 9. Effect of different parameters on the distribution of different phases and components within the aquifer after 100 days; (a) increased gas mobility; (b) increased gas injection rate; (c) comparison of plume extension for two cases with different salinity; (d) use of fresh water instead of saline brine; (e) decreased initial mole fraction of dissolved H_2S to one-fourth of the Base Case value; (f) decreased initial mole fraction of dissolved H_2S to one-eighth of the Base Case value.

(obtained by numerical integration of this graph) is equal to about 220 mol. Knowing that the molecular weight of hydrogen sulfide is equal to 34.1 kg kmol^{-1}, the molar release value noted above is equivalent to about 7.5 kg of H_2S.

4. Sensitivity analysis

Simulations were conducted to investigate the effect of flow conditions on the distribution of phases and components, and specifically to investigate the evolution of H_2S at the leading edge of the plume. Flow conditions are affected by gas mobility, gas injection rate, salinity of the brine, and initial mole fraction of dissolved H_2S. For simplicity, only the results after 100 days of injection are presented, as illustrated in Fig. 9.

4.1. Effect of gas mobility

The effect of gas mobility was examined by increasing the end point of gas relative permeability from 0.4 to 1.0 (Fig. 3, K_{rg} (Case a)). In the case of a more adverse mobility ratio (i.e., a higher gas mobility), at any given time the gas spreads over a larger contact area with the aqueous phase (larger radius of plume) in comparison with the Base Case, thereby stripping H_2S more effectively from the brine in contact with the advancing gas front (Fig. 9a). For this case, after 100 days, δ would be 1.65 m which is 0.6 m greater than the Base Case at that comparable point in time. Also note that, at that time, the gas plume itself is 5 m ahead of the Base Case model.

4.2. Effect of gas injection rate

The effect of gas injection rate was probed by increasing the injection rate from 4.0 rm^3/day to 10.0 rm^3/day. The effect of increasing the gas rate is similar to that of increasing the gas relative permeability. Needless to say, these two are different in one important aspect. Any change in relative permeability curves causes direct change in the characteristic fractional flow curve which in turn changes the phase saturation distributions. However, increasing the injection rate does not have any effect on the fractional flow curve. Instead, increasing the injection rate causes the plume to propagate faster and to contact a larger area at a specific time in comparison with the Base Case. Fig. 9b demonstrates that, after 100 days, the plume has passed 46 m. The results also reveal that the rate of increase in the width of characteristic FWHM or δ increases and reaches a value of 0.0045 m/day (similar calculation to Eq. (3)).

4.3. Effect of brine salinity

As has been pointed out by several researchers, the solubility of CO_2 and H_2S in brine will decrease with an increase in brine salinity (e.g., Enick and Klara, 1990; Duan et al., 2007). The effect of salinity was examined by considering fresh water instead of brine. It was assumed that the initial mole fraction of dissolved H_2S was equal to the saturated brine value in the Base Case (i.e., 0.02). The data in the third column of Table 1 ("Fresh water") was used in the simulation models to reflect the higher solubility of gaseous components in the fresh water. The higher solubility of the gaseous components into fresh water relative to the brine case causes the ultimate radius of the CO_2 plume to shrink from 29.3 m in the Base Case to 28.9 m in this fresh water case (see Fig. 9c). This of course means that less H_2S was released from the fresh water case (see Fig. 9d).

4.4. Effect of initial mole fraction of dissolved H_2S in brine

Simulations were run for two cases where the initial mole fraction of the dissolved H_2S in brine was substantially decreased. In the first case (Fig. 9e), the initial mole fraction of dissolved H_2S was

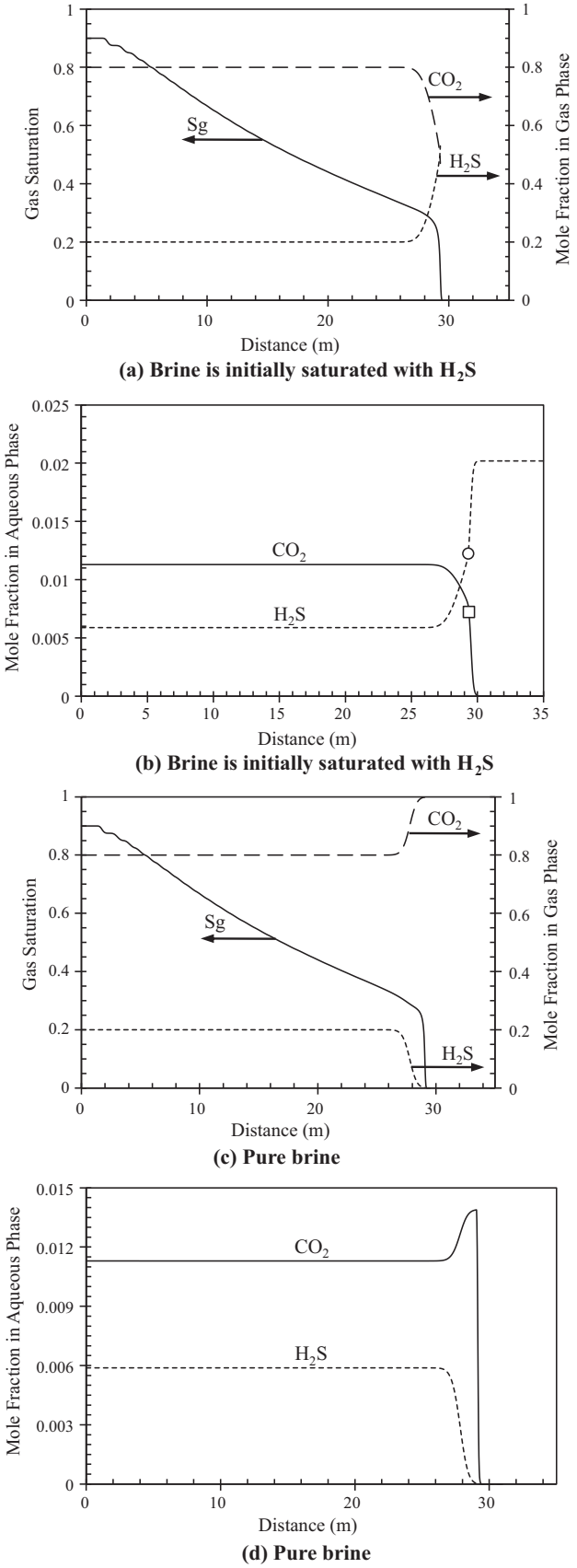

Fig. 10. Comparison between phase and component distribution for acid gas injection in two cases; (a and b) the brine is initially saturated with H_2S (where, similar to what was displayed in Fig. 6, the "○" and "□" symbols indicate the equilibrated mole fraction of H_2S and CO_2, respectively, in the aqueous phase in the last block invaded by the gas plume); (c and d) the brine is initially free of any dissolved H_2S.

equal to 0.005 and, for the second one (Fig. 9f), that initial mole fraction was equal to 0.0025 (i.e., one-fourth and one-eighth of the Base Case value, respectively). The evolution of H_2S in these cases is clearly different versus the Base Case. The brine in the Base Case is saturated with H_2S; hence, dissolution of H_2S into the aqueous phase does not occur. However, in the cases of unsaturated brine, part of the exsolved H_2S which remains as a gaseous accumulation would be consumed in the dissolution process. Therefore (at least at the gas front), dissolution and exsolution of H_2S happen simultaneously, causing significant delay in reaching the final composition for different components, meaning less H_2S is released to the gas phase.

5. Injection of acid gas into sour aquifers

Acid-gas injection operations represent a commercial-scale analogue to geological storage of CO_2, which is one of the most promising means of reducing anthropogenic CO_2 emissions into the atmosphere in the short-to-medium term (IPCC, 2007). Due to the importance of the operation, it is worth studying the impact of acid gas injection in sour aquifers and comparing these results with those of injection into pure brine (i.e., a saline aquifer with no other impurities).

Injection of a mixture of 80% CO_2 and 20% H_2S for 100 days into saline aquifers with properties in Table 2 was studied. The same simulations were repeated for brine with the same salinity but in the absence of initial dissolved H_2S.

Fig. 10a and b shows the results of the injection process in the sour aquifer. As can be seen, the injected streams strip away the dissolved H_2S and, at the same time, both CO_2 and H_2S are simultaneously seeking to attain equilibrium in the in-situ brine.

Fig. 10c and d illustrate the results associated with injection of acid gas into a saline aquifer which is initially free of any H_2S. As expected, as the gas continues its flow away from the injection well, it comes into contact with unsaturated formation water and the higher H_2S solubility in brine causes the chromatographic separation of the two gases, resulting in H_2S being stripped off at the leading edge of the gas plume (Bachu and Bennion, 2009). In this situation, the zone with high composition of H_2S in the gas plume does not appear. The depicted results in these two figures are similar to the results previously reported by Bachu et al. (2009).

6. Summary and conclusions

Compositional numerical simulations were performed to characterize the exsolution of H_2S during carbon dioxide and acid gas sequestration in saline aquifers containing pre-existing dissolved H_2S as an impurity. Simulation results confirm the formation of two distinguishable sub-regions in the volume swept by the gas plume. For pure CO_2 injection, the first sub-region is characterized by the absence of H_2S in both aqueous and gaseous phases. This sub-region occupies the interior cylindrical region centered at the injection point. On the other hand, in the outer cylindrical sub-region surrounding the first sub-region, the H_2S mole fraction gradually increases toward the leading edge of the advancing gas front. The size of the evolved sub-region increases over time. The maximum H_2S mole fraction in gas phase is affected by the reservoir conditions under investigation, including the pressure, temperature, and salinity. Since this was a characterization study, precise quantification of the results was not pursued as a goal of this study; therefore, the results would be subject to minor changes if, for example, the vaporization of water is considered.

Sensitivity analysis was performed to explore the effects of flow conditions and fluid characteristics on the sizes of these sub-regions and particularly the alteration of the H_2S mole fraction profile in the second sub-region. The study was limited to the main parameters such as gas mobility, gas injection rate, brine salinity, and initial mole fraction of dissolved H_2S impurity. Gas mobility, which is controlled by relative permeability of gas, had a direct effect on the size of the plume. Increasing the gas mobility causes the plume size to increase and consequently enhances the release of H_2S. Injection rate changes the rate of growth of the second sub-region. Brine salinity influences gas solubilities which accordingly affect the evolution of the H_2S dissolved species. Increased solubility reduces the exsolution of dissolved hydrogen sulfide. Although the initial mole fraction of dissolved H_2S has a direct effect on the amount of exsolvable H_2S, a low initial mole fraction is not a serious barrier for H_2S to reach appreciable levels near the leading edge of the plume.

Injection of a mixture of 80% CO_2 and 20% H_2S as an acid gas into a sour aquifer was also explored. The results show that, in contrast with the injection of pure carbon dioxide, the injection of the acid gas mixture is accompanied by the simultaneous exsolution and dissolution of H_2S from and into the aqueous phase. For low mole fraction of hydrogen sulfide in the injection fluid, the dissolution of this component causes no practical change in the mole fraction profile of H_2S in comparison with injection of pure CO_2 into sour saline aquifers. Injection of an acid gas mixture into an ordinary brine aquifer gives rise to the formation of sour brine in the swept region as unsaturated water easily strips away H_2S from the injected CO_2 stream.

The results of this study are important in establishing monitoring strategies at CO_2 storage sites, and in evaluating the risks associated with the possible leakage of evolved H_2S during CO_2 and acid gas injection into sour saline aquifers. This research also establishes the level of corrosivity represented by CO_2 and H_2S concentrations (affecting pH levels and partial pressures of corrosive elements, etc.) in both the aqueous and gas phases when the plume intersects wells that penetrate the injection horizon. The effect of other impurities such as CH_4, N_2, and SO_2, either as in situ components or as constituents of the injection stream, can be studied in a similar manner and should be the subject of future studies.

Acknowledgments

Financial support for this work was provided byNSERC Strategic Grant and AERI with additional funding from industry partners through Wabamun Area CO_2 Sequestration Project (WASP, http://people.ucalgary.ca/~keith/wasp.html) led by University of Calgary. Simulation software (GEM) was donated by the Computer Modelling Group. This support is gratefully acknowledged. Finally, we also wish to express our particular thanks to Drs. Pooladi-Darvish and Hassanzadeh for their extremely helpful discussions and generous suggestions for improvements to this paper.

References

Adams, J.J., Bachu, S., 2002. Equations of state for basin geofluids: algorithm review and intercomparison for brines. Geofluids 2, 257–271.

Ahmed, T., 1989. Hydrocarbon Phase Behaviour. Gulf Publishing Company, Houston.

Bachu, S., Carroll, J.J., 2005. In-situ phase and thermodynamic properties of resident brine and acid gases (CO_2 and H_2S) injected into geological formations in western Canada. In: Rubin, E.S., Keith, D.W., Gilboy, C.F. (Eds.), Proceedings of the 7th International Conference on Greenhouse Gas Control Technologies, vol. I. Elsevier, London, U.K., pp. 449–457.

Bachu, S., Gunter, W.D., 2005. Overview of acid gas injection operations in western Canada. In: Rubin, E.S., Keith, D.W., Gilboy, C.F. (Eds.), Proceedings of the 7th International Conference on Greenhouse Gas Control Technologies, vol. I. Elsevier, London, U.K, pp. 443–448.

Bachu, S., Bennion, D.B., 2009. Chromatographic partitioning of impurities contained in a CO_2 stream injected into a deep saline aquifer: Part 1. Effect of gas composition and in-situ conditions. Int. J. Greenhouse Gas Control, doi:10.1016/j.ijggc.2009.01.001.

Bachu, S., Pooladi-Darvish, M., Hong, H., 2009. Chromatographic partitioning of impurities (H_2S) contained in a CO_2 stream injected into a deep saline aquifer: Part 2. Effect of flow conditions. Int. J. Greenhouse Gas Control, doi:10.1016/j.ijggc.2009.01.002.

Battistelli, A., Marcolini, M., 2009. TMGAS: a new TOUGH2 EOS module for the numerical simulation of gas mixtures injection in geological structures. Int. J. Greenhouse Gas Control 3 (4), 481–493.

Bennion, D.B., Bachu, S., 2008. Drainage and imbibition relative permeability relationships for supercritical CO_2/brine and H_2S/brine systems in intergranular sandstone, carbonate, shale and anhydrite rocks. SPE Res. Eng. Eval. 11 (3), 487–496, doi:19.2118/99326PA.

Carrol, J.J., 2002a. Phase equilibria relevant to acid gas injection: part 1—non-aqueous phase behaviour. JCPT 41 (June (6)).

Carrol, J.J., 2002b. Phase equilibria relevant to acid gas injection: part 2—aqueous phase behavior. JCPT 41 (June (7)).

Computer Modelling Group (CMG), 2008. User's Guide-GEM: Advanced Compositional Reservoir Simulator. Version 2008.12. Computer Modelling Group Ltd., Calgary, AB, Canada.

Corey, A.T., 1954. The interrelation between gas and oil relative permeabilities. Producers Mon. (November), 38–41.

Doughty, C., Pruess, K., Benson, S.M., Freifeld, B.M., Gunter, W.D., 2004. Hydrological and geochemical monitoring for a CO_2 sequestration pilot in a brine formation. LBNL Report 55104, Lawrence Berkeley National Laboratory, Berkeley, CA.

Duan, Z., Sun, R., Liu, R., Zhu, C., 2007. Accurate thermodynamic model for the calculation of H_2S solubility in pure water and brine. Energy and Fuels 21, 2056–2065.

Enick, R.M., Klara, S.M., 1990. CO_2 solubility in water and brine under reservoir conditions. Chem. Eng. Commun. 90, 23–33.

Hovorka, S.D., Doughty, C., Holtz, M., 2004. Testing efficiency of storage in the subsurface: Frio brine pilot experiment. LBNL Report 55730, Lawrence Berkeley National Laboratory, Berkeley, CA.

Hutcheon, I., 1999. Controls on the distribution of non-hydrocarbon gases in the Alberta Basin. Bull. Canadian Petrol. Geol. 47 (4), 573–593.

Intergovernmental Panel on Climate Change (IPCC), 2007. In: Pachauri, R.K., Reisinger, A. (Eds.), Core Writing Team, Climate Change 2007: Synthesis Report. Contribution of Working Groups I, II and III to the Fourth Assessment Report of the Intergovernmental Panel on Climate Change. IPCC, Geneva, Switzerland.

Kumar, A., Ozah, R., Noh, M., Pope, G.A., Bryant, S., Sepehrnoori, K., Lake, L.W., 2005. Reservoir simulation of CO_2 storage in deep saline aquifers. SPE J. 10 (3), 336–348.

Leonenko, Y., Keith, D.W., 2008. Reservoir engineering to accelerate the dissolution of CO_2 stored in aquifers. Environ. Sci. Technol. 42, 2742–2747.

Li, Y., Nghiem, L.X., 1986. Phase equilibria of oil, gas and water/brine mixtures from a cubic equation of state and Henry's Law. Canadian J. Chem. Eng. 64 (3), 486–496.

Li, Z., Firoozabadi, A., 2009. Cubic-plus-association equation of state for water-containing mixtures: is "Cross Association" necessary? AIChE J. 55, 1803–1813.

NIST, 2007. Standard Reference Database 4. NIST Thermophysical Properties of Hydrocarbon Mixtures, Program SUPERTRAPP–Version 3.2. Gaithersburg, MD 20899, USA.

Ozah, O.C., Lakshminarasimhan, S., Pope, G.A., Sepehrnoori, K., Bryant, S.L., 2005. Numerical simulation of the storage of pure CO_2 and CO_2–H_2S gas mixtures in deep saline aquifers. SPE 97255.

Peng, D.Y., Robinson, D.B., 1976. A new two-constant equation of state. Ind. Eng. Chem. Eng. Fundam. 15, 59–64.

Pooladi-Darvish, M., Hong, H., Stocker, R.K., Bennion, D.B., Theys, S., Bachu, S., 2009. Chromatographic partitioning of H_2S and CO_2 in acid gas disposal. JCPT 48 (10), 52–57.

Pruess, K., 2009. Formation dry-out from CO_2 injection into saline aquifers: 2. Analytical model for salt precipitation. Water Resour. Res. 45, W03403, doi:10.1029/2008WR007102.

Zeidouni, M., Pooladi-Darvish, M., Keith, D.W., 2009. Analytical solution to evaluate salt precipitation during CO_2 injection in saline aquifers. Int. J. Greenhouse Gas Control 3 (5), 600–611.